p Doping in Expanded Phases of ZnO: An *Ab Initio* Study

D. Hapiuk,[1,*] Miguel A. L. Marques,[1] P. Melinon,[1] José A. Flores-Livas,[1] Silvana Botti,[1,2] and B. Masenelli[3]

[1]*Université de Lyon, F-69000 Lyon, France and Laboratoire PMCN, CNRS UMR 5586, Université de Lyon 1, F-69622 Villeurbanne Cedex, France*

[2]*Laboratoire des Solides Irradiés and ETSF, École Polytechnique, CNRS, CEA-DSM, 91128 Palaiseau, France*

[3]*Université de Lyon, F-69000 Lyon, France and Institut des Nanotechnologies de Lyon, UMR 5270 CNRS, INSA Lyon, 7 avenue Jean Capelle, 69621 Villeurbanne Cedex, France*

(Received 28 June 2011; revised manuscript received 21 November 2011; published 16 March 2012)

The issue of *p* doping in nanostructured cagelike ZnO is investigated by state-of-the-art calculations. Our study is focused on one prototypical structure, namely, sodalite, for which we show that *p*-type doping is possible for elements of the V, VI, and VII columns of the periodic table. However, some dopants tend to form dimers, thus impairing the stability of this kind of doping. This difference of behavior is discussed, and two criteria are proposed to ensure stable *p* doping.

DOI: 10.1103/PhysRevLett.108.115903 PACS numbers: 66.30.−h, 61.46.−w, 71.15.Mb, 71.20.Nr

The interest in ZnO has greatly increased over the last decade due to its remarkable properties. Its excitonic UV luminescence and high excitonic binding energy (60 meV) should enable nanometric-scaled applications such as biological tracers [1], UV laser diodes [2] and polariton lasers, or integration in solar cells with high efficiency. In this context, the electronic properties of ZnO, and more specifically the possibilities for doping, hold a particular interest. However, unlike *n*-type doping, *p*-type doping is a real problem for this material, therefore limiting its use for electronic applications. This behavior arises from a variety of causes, including native crystalline defects and impurity incorporations [3]. Many attempts have been made to *p* dope wurtzite ZnO samples, but sound achievements are scarce [4]. These difficulties could be circumvented by exploring other ZnO phases that have been proposed in recent years [5–8]. Of particular interest are cagelike structures that are particularly suited for endohedral doping. Such phases have been recently proposed for hydrogen purification membranes [9] and have been shown to exhibit a transient *p*-type doping due to the free motion of H atoms in the network [9]. Furthermore, cagelike endohedral doping has proved to be an interesting method used in other semiconductor materials. For instance, in Si clathrates, endohedral doping by alkaline atoms allows the control of the electronic properties [10] up to the appearance of superconductivity [11]. It is thus relevant to investigate the possibilities of endohedral doping in ZnO cagelike materials in the hope to achieve *p* doping.

In this Letter, we investigate the endohedral *p* doping of a particular ZnO cagelike structure, namely, the sodalite structure (SOD, according to the nomenclature of the International Zeolite Association). This turns out to be the simplest and most symmetric binary structure of the cagelike family and is the unique solution to the Kelvin problem for binary compounds [12]. It consists of a regular stacking of truncated octahedra which are Archimedean solids with 14 faces (8 regular hexagons and 6 squares) leading to the net formula $(ZnO)_{12}$ (see inset in Fig. 1). Furthermore, even though the ZnO sodalite structure has not been experimentally synthesized, theoretical [13] and experimental works [14] tend to show that its building block, the $(ZnO)_{12}$ cluster, is stable and energetically favored. Furthermore, a 25% cosubstituted cagelike structure (the ATN phase, according to the nomenclature of the International Zeolite Association) has been obtained by a solid-state reaction [15]. These results point to the possibility of growing cagelike expanded phases of II–VI semiconductors and, in particular, of ZnO.

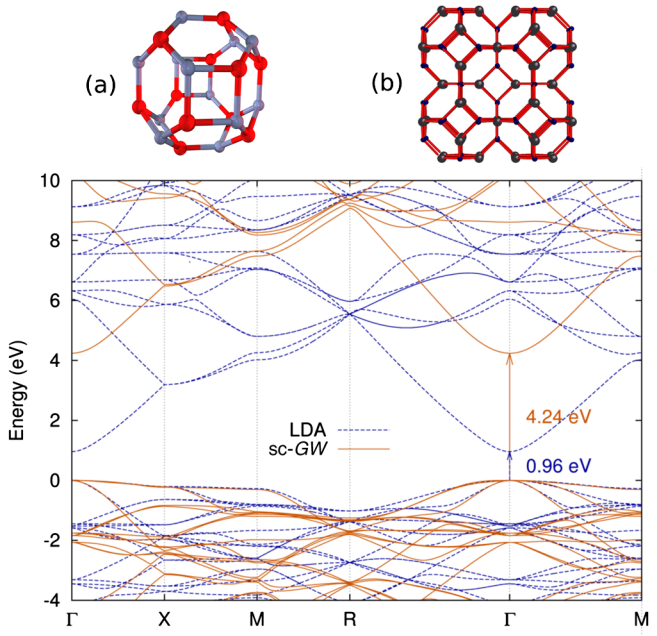

FIG. 1 (color online). Band structure of ZnO sodalite structure in DFT LDA and sc-*GW*. The gap is direct at Γ and estimated to be 4.2 eV in sc-*GW* and 0.9 eV in LDA. (a) presents an elementary cage of the sodalite illustrated in (b).

To study the stability and the electronic structure of sodalite, we used first-principles calculations within the density-functional theory (DFT) formalism and with a plane-wave pseudopotential approach (using the VASP code [16]). We used the Perdew-Burke-Ernzerhof exchange-correlation functional [17] and the projector augmented-wave description of the electron-ion interaction [18]. Brillouin zone integrals were converged with a 600 eV plane-wave cutoff and a $2 \times 2 \times 2$ Monkhorst-Pack k-point mesh, using the tetrahedron method with Blöchl corrections. The relaxation was performed with the standard conjugated gradient algorithm. This calculation procedure is common to all the results presented in this Letter, unless otherwise stated.

From all known cagelike ZnO structures [8], the sodalite has a relatively low energy, with a cohesion energy of -8.972 eV per unit of ZnO (see Table I), when calculated as the difference between the energy of sodalite and of isolated atoms. It is 132 meV higher than the energy of wurtzite but also 165 meV lower than that of rocksalt, the latter structures being the only naturally occurring phases. This result is consistent with previous calculations [9] and further justifies the choice of the sodalite as a potential candidate for the study of endohedral p doping.

It is true that the *ab initio* determination of the quasiparticle band structure of ZnO poses quite a complicated problem, as standard methods, such as DFT or even standard (perturbative) G_0W_0, yield band gaps that are much smaller than the experimental value [20,21]. To obtain the best possible band structure for the ZnO sodalite (cf. Figure 1), we have to go beyond these methods [22,23]. In this work, we used a state-of-the-art approach based on a restricted self-consistent (sc) GW scheme. Such an approach, which we will refer to as sc-GW, consists of performing a self-consistent GW calculation within the Coulomb-hole-plus-screened-exchange approximation, followed by a perturbative GW step on top of it [24]. This method has been applied to many transition-metal compounds, yielding excellent results for the band gaps and the quasiparticle band structure [24–27]. The sc-GW calculations were performed using the code ABINIT [28]. We included semicore states in the valence to build the norm-conserving pseudopotentials for Zn and used a $3 \times 3 \times 3$ sampling of the Brillouin zone. The absolute value of the sc-GW direct band gap at Γ has, however, to be interpreted with care. In fact, for wurtzite ZnO (experimental gap 3.3 eV), our method yields a direct band gap at Γ of 4.4 eV, while the local-density approximation (LDA) yields 0.82 eV and standard GW 2.1 eV. The overestimation of the gap by sc-GW can probably be explained by the neglect of the contribution of phonons to the screening, which can have a very large effect in ionic oxide materials [27,29]. On the other hand, for ZnO sodalite, we obtain a sc-GW direct band gap at Γ of 4.2 eV (Fig. 1), while LDA yields 0.96 eV and standard G_0W_0 2.5 eV. By comparing the two structures, and by assuming that sc-GW is our best theoretical estimate, it becomes clear that the experimental gap of ZnO sodalite is direct at Γ and is very likely lower than the one of the wurtzite structures by 0.1–0.3 eV, i.e., in the range of 3.2–3.4 eV. The ZnO sodalite thus retains the interesting feature of the wurtzite ZnO for the UV optoelectronic applications and motivates the study of its doping properties.

To study p doping, we used elements of the V, VI, and VII columns of the periodic table, with atomic concentrations of the doping element varying from 1% to 14% (i.e., every cage is filled). Table II presents the cohesion energies of the ZnO sodalite doped with different dopants for a 7% concentration (i.e., every other cage is filled). The doped ZnO sodalite is always more stable than the undoped one, indicating hybridization with the dopant. With F, the absolute value of the cohesion energy of the structure reaches the maximum of 335 meV/ZnO higher than the undoped ZnO sodalite. This result indicates that the dopant could be useful to ease the synthesis of the ZnO sodalite, just as it is the case

TABLE I. Cohesion energy difference ΔE and volume for several cagelike structures [5–8] as named by the International Zeolite Association and obtained from DFT calculations. The lattice and coordinate parameters were obtained from Ref. [19].

Name	Space group	ΔE (eV/ZnO)	Volume (Å^3/ZnO)
Wurtzite	$P63mc$	0	24.85
SOD	$Pm\bar{3}n$	+0.132	30.42
BCT	$I4/mmm$	+0.029	25.99
ATV	$Abm2$	+0.137	26.38
AFI	$P6cc$	+0.189	30.61
LTA	$Pm\bar{3}m$	+0.248	36.87
ATN	$I4/mmm$	+0.277	26.56
VFI	$P63/mcm$	+0.291	37.34
Rocksalt	$Fm3m$	+0.297	20.43

TABLE II. Cohesion energy of 7% doped ZnO sodalite and features of 1% doped ZnO sodalite, including the presence of the Jahn-Teller effect (JT), the proportion of hybridization at the Fermi level, and the presence of dimerization.

Dopant	E_{cohesion}(eV/ZnO)	JT	Hybrid	Dimerization
O	−9.393	Yes	26.1%	No
F	−9.439	Yes		No
Cl	−9.171	No		No
Br	−9.067	No		No
Te	−9.072	No	43.8%	No
I	−8.939	No		No
H	−9.130	Yes	20.1%	Yes
N	−9.293	Yes	37.8%	Yes
P	−9.194	No	47.7%	Yes
S	−9.173	No	45.3%	Yes
Se	−9.136	Yes	46.9%	Yes

for Si clathrates [30]. The cohesion energy naturally varies with regard to the nature of the dopant (Table II).

Clearly, the electronic properties are also dependent on the dopant. Figure 2 presents the density of states (DOS) of the undoped ZnO sodalite along with the DOS of the structure doped with N, Cl, and Te. In all cases, the dopant atomic concentration is nearly 1% [N@$(ZnO)_{48}$, Te@$(ZnO)_{48}$, and Cl@$(ZnO)_{48}$]. All are p-type doped, as it is well evidenced by the position of the Fermi level at 0 eV. In the case of N- and Te-doped ZnO sodalite, the total electronic DOS at this particular point has an equal contribution from O and N (or Te) states and a smaller contribution from Zn states. The proportion of hybridization of the states at the Fermi level has also been calculated. This proportion has been defined as the ratio of the DOS projected on the dopant states with the total DOS at the Fermi level. A value of 0% or 100% means a pure transfer of electrons from the dopant to the electronic states of the ZnO network. This scheme is close to the conventional scheme of a hydrogenlike impurity in substitutional doping. Conversely, a value around 50% means a strong hybridization between the orbitals of the dopant and the network. The results are presented in Table II. Interestingly, all values are close to 50%, which implies that the insertion of the dopant in the ZnO sodalite cages induces a strong hybridization. As for the Cl-doped ZnO sodalite, it presents a degenerate state. This means that the dopant concentration is high enough to strongly perturb the electronic DOS of the doped sodalite. This latter is no longer a classic doped semiconductor but presents a metallic behavior. This transition is also known as the Mott transition [31] and occurs for a critical dopant concentration. Thus, the hybridization is very strong and perturbs the valence band near the Fermi level. Naturally, the critical concentration for the Mott transition depends on the nature of the dopant.

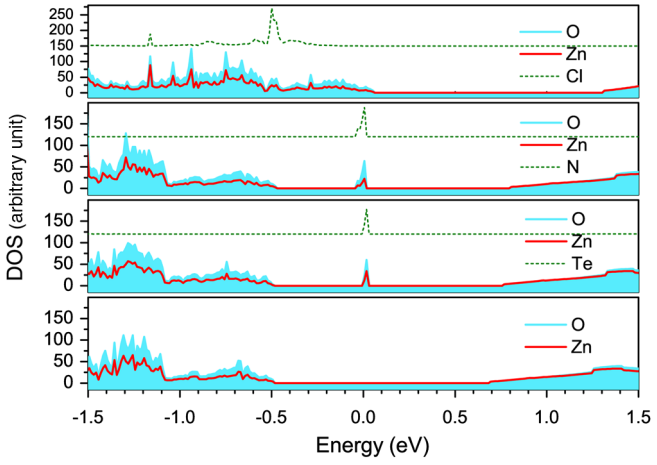

FIG. 2 (color online). Electronic density of states of N-, Cl-, and Te-doped ZnO sodalite projected on the states of the constituents. The Fermi level is located at 0 eV. The contribution of each atom is, respectively, Zn [shaded (blue) areas]; O [solid (red) lines]; and N, Te, and Cl [dotted (green) lines]. The dopant states are strongly localized near the top of the valence band. The DOS of pure ZnO sodalite is pictured in the bottom panel. The DOS of the different conduction bands has been multiplied (× 10) for the sake of visibility as well as the contribution of Cl (× 5). The dopant atomic concentration is 1%.

It is also pertinent to study the constraints induced by the dopant on the framework. For example, the equilibrium position of the Te atom is at the center of the cage and the lattice is only slightly affected by doping. Indeed, according to our calculations, the diameter of a cage of the undoped ZnO sodalite is 6.34 Å against 6.47 Å for the Te-doped one. On the contrary, the N atom moves spontaneously away from the center of the cage, exhibiting a Jahn-Teller effect, leading to an equilibrium position shifted by 1.37 Å and a lattice more deformed locally around the dopants (the cage containing the dopant is deformed, and its diameter varies between 6.16 and 6.55 Å). The shifted distance due to the Jahn-Teller effect is of the same order of magnitude as the one reported for the Na@Si_{28} silicon clathrate [10].

We also performed calculations for several other p-type dopants, as listed in Table II. For ZnO sodalite doped with Cl, Br, and I, a dopant concentration of 1% is already enough to lead to a degenerate semiconductor with the Fermi level localized in the valence band. For the other dopants, the Mott transition appears at higher concentrations. We also notice a Jahn-Teller effect for the light elements, i.e., H, N, O, and F. The inspection of the lattice distortion around the atoms that present a Jahn-Teller effect reveals a repulsion between O and the dopant, while Zn atoms remain at their initial positions.

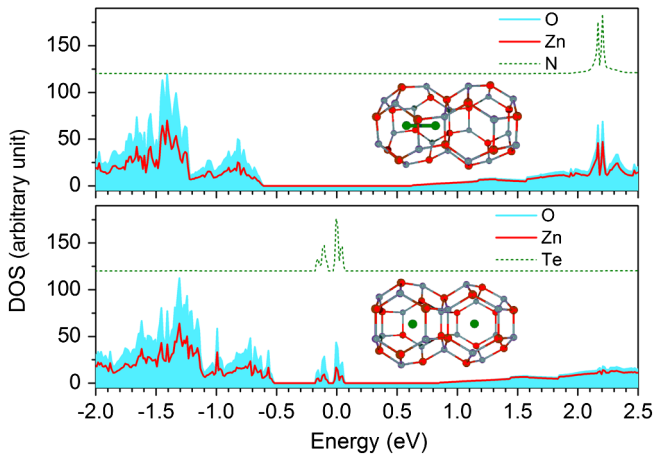

FIG. 3 (color online). Electronic density of states of N- and Te-doped ZnO sodalite projected on the states of the constituents. The Fermi level is located at 0 eV. Two dopants are placed in two neighboring cages of the ZnO sodalite, and the insets illustrate the position of the atoms after relaxation. The DOS of the different conduction bands has been multiplied (× 5) for the sake of visibility as well as the contribution of the N and Te dopants (× 2). The dopant atomic concentration is 2%.

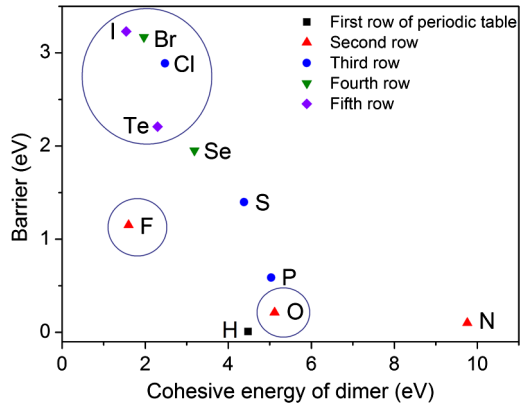

FIG. 4 (color online). Magnitude of the energy barrier in doped ZnO sodalite as a function of the cohesion energy of the dimer. The circled areas enclose the dopants which do not dimerize. Each symbol corresponds to a different row of the periodic table.

Since two adjacent cages may be occupied by doping atoms, it may be possible that those atoms dimerize. Figure 3 displays the case of Te and N doping. For that purpose, we start with two atoms in two adjacent cages [the dopant atomic concentration is thus 2%, with the stoichiometry $N@(ZnO)_{24}$] and relax the system with the conjugated gradient algorithm. As a result, Te stays at the center of the cage while N moves spontaneously to form a N_2 dimer. In the latter case, we obtain a set of two independent lattices formed by the ZnO sodalite and N_2 molecules. This is well evidenced by the sharp peaks in the DOS due to N in the conduction band far away from the Fermi level. Thus, the ZnO sodalite is not p-doped any more. The new equilibrium state exhibits a mean distance of $d_{N\text{-}N} = 1.11$ Å, close to the experimental bond length of the dimer $d_{N\text{-}N} = 1.10$ Å. This result can be obtained for other elements, like H, N, P, S, and Se, while O, F, Cl, Br, Te, and I do not dimerize and preserve p-like doping at any concentration.

Eventually, the diffusion of the dopant is of utmost importance for the ZnO sodalite synthesis. To study this problem, we calculated the magnitude of the energy barrier when the dopant moves along the [111] direction crossing the shared hexagon; see Fig. 4. The magnitude of the energy barrier is calculated between the equilibrium position of the dopant and the position where the dopant crosses the hexagonal face separating two cages. Globally, the energy barrier increases with the atom size, in agreement with steric hindrance. However, this is not the only criterion. One has also to consider the magnitude of the interaction of the guest atom with the host lattice. The interaction becomes stronger as the p valence shell of the guest atom is filled, requiring the transfer of fewer electrons to fulfill the octet rule. Considering elements belonging to the same row of the periodic table, for instance, N, O, and F, one can see that the magnitude of the energy barrier increases from N to F, almost independently of the atomic radius. The elements which do not dimerize (circled areas in Fig. 4) exhibit a high value for the energy barrier and a weak cohesion energy of the dimer. These two criteria allow us to discriminate the dopants that dimerize from those that do not. Consequently, these criteria can predict a stable or unstable p-type doping. The case of O is an exception, since, in spite of the large cohesion energy of its dimer and the small value of the energy barrier, it does not dimerize. The absolute energy barrier is relatively large compared to the thermal energy and questions the efficiency of the diffusion. We did the same calculations for the Na-doped silicon type II clathrate where diffusion is observed at moderate temperature ($T < 600$ K) [32]. This energy barrier is estimated to be 2.14 eV, similar to the ones found in ZnO sodalite.

In conclusion, using state-of-the-art DFT calculations, we showed that endohedral doping of cagelike structures is a promising method for the achievement of p doping in ZnO, even up to degenerate levels. Since doping in endohedral sites induces less stress than substitutional doping, all elements of the V, VI, and VII columns of the periodic table are eligible. However, some of them dimerize and therefore do not lead to p doping. In particular, the case of N, which is thoroughly discussed in the literature in the context of substitutional doping, does not seem to be the best candidate for endohedral doping. Other elements, such as O, F, Cl, Br, Te, and I, are, however, good possible candidates. To ensure p doping, an argument based on the balance between the cohesion energy of the dimers and the energy barrier for diffusion of the dopant is detailed. We believe that the achievement of p doping as studied in this Letter is not restricted to the particular case of the ZnO sodalite but can be generalized to other cagelike ZnO nanomaterials.

*dimitri.hapiuk@univ-lyon1.fr

[1] H. Hong, J. Shi, Y. Yang, Y. Zhang, J. W. Engle, R. J. Nickles, X. Wang, and W. Cai, Nano Lett. **11**, 3744 (2011).
[2] S. Chu, G. Wang, W. Zhou, Y. Lin, L. Chernyak, J. Zhao, J. Kong, L. Li, J. Ren, and J. Liu, Nature Nanotech. **6**, 506 (2011).
[3] Ü. Özgür, Ya. I. Alivov, C. Liu, A. Teke, A. Reshchikov, S. Doğan, V. Avrutin, S. J. Cho, and H. Morkoç, J. Appl. Phys. **98**, 041301 (2005).
[4] T. Tsukazaki, A. Ohtomo, T. Onuma, M. Ohtani, T. Makino, M. Sumiya, K. Ohtani, S. F. Chichibu, S. Fuke, Y. Segawa, H. Ohno, H. Koinuma, and M. Kawasaki, Nature Mater. **4**, 42 (2004).
[5] B. J. Morgan, Phys. Rev. B **80**, 174105 (2009).
[6] A. J. Kulkarni, M. Zhou, K. Sarasamak, and S. Limpijumnong, Phys. Rev. Lett. **97**, 105502 (2006).
[7] J. Carrasco, F. Illas, and S. T. Bromley, Phys. Rev. Lett. **99**, 235502 (2007).

[8] M. A. Zwijnenburg, F. Illas, and S. T. Bromley, Phys. Rev. Lett. **104**, 175503 (2010).
[9] D. Stradi, F. Illas, and S. T. Bromley, Phys. Rev. Lett. **105**, 045901 (2010).
[10] F. Tournus, B. Masenelli, P. Melinon, D. Connetable, X. Blase, A. M. Flank, P. Lagarde, C. Cros, and M. Pouchard, Phys. Rev. B **69**, 035208 (2004).
[11] D. Connetable, V. Timoshevskii, B. Masenelli, J. Beille, J. Marcus, B. Barbara, A. M. Saitta, G.-M. Rignanese, P. Melinon, S. Yamanaka, and X. Blase, Phys. Rev. Lett. **91**, 247001 (2003).
[12] D. Weaire and R. Phelan, Philos. Mag. Lett. **69**, 107 (1994).
[13] B. Wang, X. Wang, and J. Zhao, J. Phys. Chem. C **114**, 5741 (2010).
[14] A. Dmytruk, I. Dmytruk, I. Blonsky, R. Belosludov, Y. Kawazoe, and A. Kasuya, Microelectron. J. **40**, 218 (2009).
[15] R. Hoppe and E. Siepp, J. Solid State Chem. **72**, 52 (1988).
[16] G. Kresse and J. Furthmüller, Comput. Mater. Sci. **6**, 15 (1996).
[17] J. P. Perdew, K. Burke, and M. Ernzerhof, Phys. Rev. Lett. **77**, 3865 (1996).
[18] P. E. Blochl, Phys. Rev. B **50**, 17 953 (1994).
[19] A. A. Demkov, O. F. Sankey, J. Gryko, and P. F. McMillan, Phys. Rev. B **55**, 6904 (1997).
[20] C. Friedrich, M. C. Müller, and S. Blügel, Phys. Rev. B **83**, 081101(R) (2011).
[21] M. Stankovski, G. Antonius, D. Waroquiers, A. Miglio, H. Dixit, K. Sankaran, M. Giantomassi, X. Gonze, M. Côté, and G.-M. Rignanese, Phys. Rev. B **84**, 241201(R) (2011).
[22] M. Shishkin and G. Kresse, Phys. Rev. B **75**, 235102 (2007).
[23] A. R. H. Preston, A. DeMasi, L. F. J. Piper, K. E. Smith, W. R. L. Lambrecht, A. Boonchun, T. Cheiwchanchamnangij, J. Arnemann, M. van Schilfgaarde, and B. J. Ruck, Phys. Rev. B **83**, 205106 (2011).
[24] F. Bruneval, N. Vast, and L. Reining, Phys. Rev. B **74**, 045102 (2006).
[25] J. Vidal, F. Trani, F. Bruneval, M. A. L. Marques, and S. Botti, Phys. Rev. Lett. **104**, 136401 (2010).
[26] J. Vidal, S. Botti, P. Olsson, J.-F. Guillemoles, and L. Reining, Phys. Rev. Lett. **104**, 056401 (2010).
[27] J. Vidal, F. Trani, F. Bruneval, M. A. L. Marques, and S. Botti, Phys. Rev. Lett. **104**, 136401 (2010).
[28] X. Gonze, G.-M. Rignanese, M. Verstraete, J.-M. Beuken, Y. Pouillon, R. Caracas, F. Jollet, M. Torrent, G. Zerah, M. Mikami, Ph. Ghosez, M. Veithen, J.-Y. Raty, V. Olevano, F. Bruneval, L. Reining, R. Godby, G. Onida, D. R. Hamann, and D. C. Allan, Z. Kristallogr. **220**, 558 (2005).
[29] F. Trani, J. Vidal, S. Botti, and M. A. L. Marques, Phys. Rev. B **82**, 085115 (2010).
[30] J. S. Kasper, P. Hagenmuller, M. Pouchard, and C. Cros, Science **150**, 1713 (1965).
[31] V. I. Smelyansky and J. S. Tse, Chem. Phys. Lett. **264**, 459 (1997).
[32] A. Ammar, C. Cros, M. Pouchard, N. Jaussaud, J. M. Bassat, G. Villeneuve, M. Duttine, M. Ménétrier, and E. Reny, Solid State Sci. **6**, 393 (2004).